DOI: 10.1002/ejic.200600958

Cyanido-Bridged Dimetallic Complexes Derived from Manganese(III) Schiff Bases and Pentacyanidonitrosylchromate(I): Synthesis, Crystal Structure and Magnetic Properties

Zhong-Hai Ni,[a] Lei Zheng,[a] Li-Fang Zhang,[a] Ai-Li Cui,[a] Wei-Wei Ni,[a] Chong-Chao Zhao,[a] and Hui-Zhong Kou*[a]

Keywords: Cyanide ligands / Bridging ligands / Magnetic properties / Manganese / Schiff-base ligands

Four cyanido-bridged Mn^{III}–Cr^{I} heterodimetallic complexes have been synthesized by the reactions of Mn^{III} Schiff-base complexes with the $[Cr(CN)_5(NO)]^{3-}$ building block. X-ray diffraction analysis reveals that $[Mn(5\text{-Cl-salen})(H_2O)_2][Mn_2(5\text{-Cl-salen})_2(H_2O)_{1.5}Cr(CN)_5(NO)]$ (**1**) has a trinuclear structure, and $[Mn_3(salen)_3(H_2O)(CH_3CN)Cr(CN)_5(NO)]\cdot 0.5CH_3CN\cdot 0.5MeOH\cdot 2H_2O$ (**2**) and $[Mn(5\text{-Br-salen})(H_2O)(CH_3OH)][Mn_2(5\text{-Br-salen})_2(CH_3OH)Cr(CN)_5(NO)]\cdot 2H_2O$ (**3**) have novel 1D chain topological structures, whereas $[\{Mn(saltmen)\}_4Cr(CN)_5(NO)]ClO_4\cdot 3H_2O$ (**4**) displays a 2D layered network structure. Magnetic measurements show that the magnetic interaction between the Mn^{III} and Cr^{I} ions bridged by a cyanido group is antiferromagnetic for complexes **1**–**4**. The magnetic fitting for the trinuclear complex **1** gives the magnetic coupling constant $J = -10.4(1)$ cm^{-1} and $J' = -1.29(2)$ cm^{-1} based on the isotropic Hamiltonian $\hat{H} = -2J\hat{S}_{Cr}[\hat{S}_{Mn(1)} + \hat{S}_{Mn(2)}] - 2J'\hat{S}_{Mn(1)}\hat{S}_{Mn(2)}$. Complex **2** exhibits 3D antiferromagnetic ordering ($T_N = 3.5$ K) with a metamagnetic character below T_N. Complex **3** exhibits an obvious frequency-dependent AC magnetic susceptibility below 4.0 K, which is due to the spin-glass behavior. The layered complex **4** displays 3D ferromagnetic ordering with $T_c = 6.4$ K due to the ferromagnetic interaction between the ferrimagnetic layers.

Introduction

In the past two decades, the design and synthesis of cyanido-bridged molecule-based magnetic materials with high-T_c, single-molecule magnets (SMMs), single-chain magnets (SCMs), and those that exhibit spin crossover (SCO) or photomagnetic behavior has become one of the most important fields in coordination chemistry and magnetochemistry.[1–10] (Schiff base)Mn^{III} complexes and hexacyanidometalate building blocks have been shown to be two intriguing precursors for the above purpose. Indeed, their combinations have successfully yielded a variety of structures, including polynuclear[3b,11–18] 1D chains[19,20] and 2D networks,[11,12,21–23] by tuning the Schiff-base ligands and the coordination numbers around the Mn^{III} ion. However, much attention has been paid to the investigation of Mn^{III}–Fe^{III} complexes derived from (Schiff base)Mn^{III} complexes and $[Fe(CN)_6]^{3-}$, and only limited examples have been obtained based on (Schiff base)Mn^{III} complexes and other cyanido-containing building blocks.[7,17,18,24–30] In particular, to the best of our knowledge, there is still no report on cyanido-bridged Mn^{III}–Cr^{I} or Mn^{III}–Cr^{III} 1D chain-like complexes and only three known Mn^{III}–Fe^{III} 1D assemblies,[19,20,25] one Mn^{III}–Mn^{III}, and one Mn^{III}–Mo^{IV} 1D chain complex[24,26] derived from (Schiff base)Mn^{III} complexes and $[Fe(CN)_6]^{3-}$, $[Fe(bpb)(CN)_2]^{-}$, $[Mn(salen)(CN)_2]^{-}$, or $[Mo(CN)_8]^{4-}$ building blocks.

In light of our continuing interest in cyanido-bridged dimetallic complexes, we are interested in extending this system to the paramagnetic $[Cr(CN)_5(NO)]^{3-}$ building block, which has the same negative charge as $[M^{III}(CN)_6]^{3-}$ (M = Fe, Cr, Co or Mn). In addition, the unpaired electron (d^5, low-spin) in Cr^{I} means that it has the same low spin as the Fe^{III} ion ($S = 1/2$), and is different from the Cr^{III} ion ($S = 3/2$). Therefore, special interest lies in comparing the magnetic properties of $[Cr(CN)_5(NO)]^{3-}$ with $[Fe(CN)_6]^{3-}$ and in the search for a new family of molecule-based magnets. To this end, we decided to investigate complexes based on $[Cr(CN)_5(NO)]^{3-}$ and (Schiff base)Mn^{III} building blocks. Herein, we report the synthesis, crystal structures, and magnetic properties of four such complexes, including the trinuclear complex $[Mn(5\text{-Cl-salen})(H_2O)_2][Mn_2(5\text{-Cl-salen})_2(H_2O)_{1.5}Cr(CN)_5(NO)]$ (**1**) and two novel 1D chain complexes $[Mn_3(salen)_3(H_2O)(CH_3CN)Cr(CN)_5(NO)]\cdot 0.5CH_3CN\cdot 0.5MeOH\cdot 2H_2O$ (**2**), and $[Mn(5\text{-Br-salen})(H_2O)(CH_3OH)][Mn_2(5\text{-Br-salen})_2(CH_3OH)Cr(CN)_5(NO)]\cdot 2H_2O$ (**3**), as well as one 2D layered compound $[\{Mn(saltmen)\}_4Cr(CN)_5(NO)]ClO_4\cdot 3H_2O$ (**4**), [salen^{2-} = *N*,*N*′-ethylenebis(salicylideneaminato) dianion, 5-Br-salen^{2-}

[a] Department of Chemistry, Tsinghua University, Beijing, Beijing 100084, China
Fax: +86-10-62771748
E-mail: kouhz@mail.tsinghua.edu.cn

Supporting information for this article is available on the WWW under http://www.eurjic.org or from the author.

= *N*,*N*′-ethylenebis(5-bromosalicylideneaminato) dianion, 5-Cl-salen^{2-} = *N*,*N*′-ethylenebis(5-chlorosalicylideneaminato) dianion, and saltmen^{2-} = *N*,*N*′-(1,1,2,2-tetramethylethylene)bis(salicylideneaminato) dianion].

Results and Discussion

Synthesis and General Characterization

The reaction between the different (Schiff base)Mn^{III} complexes {[Mn(salen)]ClO_4, [Mn(5-Cl-salen)]ClO_4, [Mn(5-Br-salen)]ClO_4, or [Mn(saltmen)]ClO_4} and $K_3Cr(CN)_5(NO)$ gave entirely different molecular structures under similar conditions. Complex **1**, for example, has an Mn_2Cr trinuclear structure with a monomer (Schiff base)Mn^{III} complex as the balanced cation, whereas complexes **2** and **3** have 1D topological structures (Scheme 1) with a 3:1 alternating arrangement of Mn^{III} and Cr^{I}. Complex **4** is a 2D network in which the (Schiff base)Mn^{III} complex forms an out-of-plane dimeric motif with a biphenolate bridge, which is similar to that of the previously reported complexes [{Mn(saltmen)}$_4${Fe(CN)$_6$}]ClO_4·H_2O,[12] $(Et_4N)[Mn_2(5\text{-}MeOsalen)_2Fe(CN)_6]$[20] [5-MeOsalen^{2-} = *N*,*N*′-ethylenebis(5-methoxysalicylideneiminate)] and [Mn(salen)(H_2O)$_2$]$_2$[{Mn(salen)(H_2O)}{Mn(salen)}$_2${Mo(CN)$_8$}]·0.5ClO_4·0.5OH·4.5H_2O.[26] It is intriguing to note that the formation of different cyanido-bridged Mn^{III}–Cr^{I} complexes is a very subtle process, which further shows that the steric effects of the Schiff-base ligands play an important role in the self-assembly of Mn^{III}–M (M = Fe^{III}, Cr^{III} and Cr^{I}) complexes.

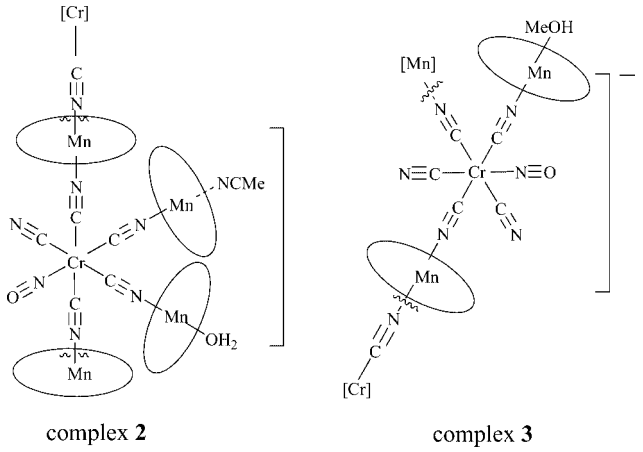

Scheme 1. Schematic representation of the chain-like structures in **2** and **3**. The circles represent salen^{2-} and 5-Br-salen^{2-} for **2** and **3**, respectively.

The IR spectra in the range 2100–2140 cm^{-1} exhibit moderately sharp peaks assigned to cyanido stretching absorptions. The weak peaks at 1677–1712 cm^{-1} can be attributed to the N=O stretching vibration in these complexes. For complex **4**, the strong broad peaks centered at around 1090 cm^{-1} suggest the presence of ClO_4^- anions in the complex.

Crystal Structures

Complex **1** consists of two crystallographically independent trinuclear [{Mn(5-Cl-salen)}$_2$Cr(CN)$_5$(NO)]$^-$ units with two free [Mn(5-Cl-salen)(H_2O)$_2$]$^+$ units as charge-balancing cations. The two [Mn(5-Cl-salen)]$^+$ segments are bound at the *cis* positions of the central Cr^{I} ion through two *cis* cyanido groups (see Figure 1 and Table 1).

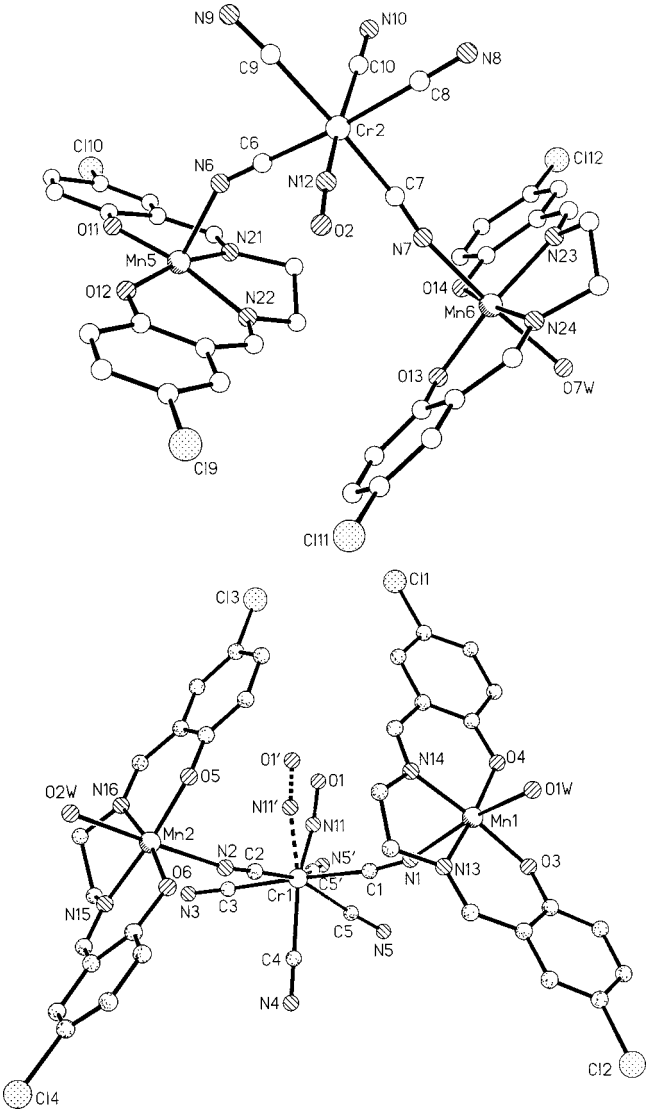

Figure 1. Structure of two Mn_2Cr trinuclear anionic units in compound **1**.

Three Mn^{III} ions in the trinuclear units are ligated by three nitrogen atoms from the 5-Cl-salen^{2-} ligand and the cyanido bridge and three oxygen atoms from the Schiff-base ligand and the coordinated water molecule to give a distorted MnN_3O_3 octahedral environment. One Mn^{III} ion is pentacoordinated by two Schiff-base nitrogen and two Schiff-base oxygen atoms as well as one cyanido nitrogen atom to yield a square-pyramidal MnN_3O_2 environment, which weakly interacts with a phenoxy oxygen atom [O(7)$^{\#}$] from an adjacent free (Schiff base)Mn^{III} unit (symmetry operation: $^{\#}$ –2/3 + *x*, –1/3 + *y*, 2/3 + *z*) with an

Table 1. Selected bond lengths [Å] and angles [°] for complex **1**.[a]

Mn(1)–N(1)	2.264(6)	Mn(2)–N(2)	2.229(11)	Mn(3)–N(17)	1.985(6)
Mn(1)–N(13)	1.980(7)	Mn(2)–N(15)	1.975(11)	Mn(3)–N(18)	1.964(6)
Mn(1)–N(14)	1.952(8)	Mn(2)–N(16)	2.017(10)	Mn(3)–O(7)	1.890(5)
Mn(1)–O(3)	1.886(6)	Mn(2)–O(5)	1.861(11)	Mn(3)–O(8)	1.876(5)
Mn(1)–O(4)	1.893(5)	Mn(2)–O(6)	1.916(9)	Mn(3)–O(3w)	2.267(5)
Mn(1)–O(1w)	2.291(5)	Mn(2)–O(2w)	2.236(6)	Mn(3)–O(4w)	2.306(5)
Mn(4)–N(19)	1.980(7)	Mn(5)–N(6)	2.131(6)	Mn(6)–N(7)	2.214(7)
Mn(4)–N(20)	1.983(6)	Mn(5)–N(21)	1.952(6)	Mn(6)–N(23)	1.993(7)
Mn(4)–O(9)	1.873(5)	Mn(5)–N(22)	1.982(6)	Mn(6)–N(24)	1.990(7)
Mn(4)–O(10)	1.888(5)	Mn(5)–O(11)	1.873(5)	Mn(6)–O(13)	1.904(6)
Mn(4)–O(5w)	2.226(5)	Mn(5)–O(12)	1.952(6)	Mn(6)–O(14)	1.881(6)
Mn(4)–O(6w)	2.240(5)	Mn(5)–O(7)$^{\#1}$	3.369(5)	Mn(6)–O(7w)	2.235(7)
Mn(1)–N(1)–C(1)	156.5(6)	Mn(2)–N(2)–C(2)	161.9(11)	Mn(5)–N(6)–C(6)	147.4(6)
Mn(6)–N(7)–C(7)	169.3(6)				

[a] Symmetry operation: $^{\#1}$ –2/3 + *x*, –1/3 + *y*, 2/3 + *z*.

Mn(5)–O(7)$^{\#}$ bond length of 3.369(5) Å. The two discrete Mn^{III} ions are coordinated by the Schiff-base ligand and two water molecules to form a distorted octahedral MnN_2O_4 environment. The Mn–$N_{cyanido}$ bond lengths vary from 2.131(6) to 2.264(6) Å. The Mn–N≡C bonds are bent [147.4(6)–168.3(6)°], with an average bond angle of 158.7(6)°. The shortest intramolecular Mn···Cr separation through the bridging cyanido ligand is 5.125 Å, and the shortest intermolecular metal–metal distance is 6.388 Å for Mn···Cr.

The cell-packing diagram of complex **1** (see Supporting Information) shows an H-bonding interaction between the two O atoms of one 5-Cl-salen^{2-} ligand and a coordinated water molecule as well as between a cyanido nitrogen atom and a coordinated water molecule. Interestingly, the cell packing along the *c* axis is highly ordered, with many honeycomb holes in which all the chlorine atoms from the Schiff-base ligands face the center of the holes.

The structure of complex **2** consists of a neutral chain which is formed by a $[Cr(CN)_5(NO)]^{3-}$ and three $[Mn(salen)]^+$ units connected by cyanido ligands (Figure 2). Four cyanido ligands of $[Cr(CN)_5(NO)]^{3-}$ coordinate axially to the $[Mn(salen)]^+$ units. The primary chain is composed of alternate Cr(1) and Mn(1) units bridged by two *trans*-cyanido groups in $[Cr(CN)_5(NO)]^{3-}$. Two $[Mn(salen)]^+$ units [Mn(2) and Mn(3)] dangle outside the primary $Mn^{III}Cr^{I}$ chain. One dangling $[Mn(salen)]^+$ unit has a distorted octahedral environment with an acetonitrile nitrogen atom hemicoordinated [Mn(2)–N(13) 2.605(5) Å]. Each Mn^{III} ion is hexacoordinate and has a distorted octahedral surrounding [MnN_3O_3 for Mn(2) and Mn(3), and MnN_4O_2 for Mn(1)] due to the Jahn–Teller effect for a high-spin d^4 Mn^{III} ion. The Mn–$N_{cyanido}$ bonds are comparatively long, ranging from 2.206(3) to 2.333(3) Å. The Cr^{I} ion lies in a compressed CrC_5N octahedral geometry, as evidenced by the shorter Cr–N bond [1.695(3) Å for Cr(1)–N(6)] than the Cr–C distance [2.049(4)–2.111(3) Å], which is very different from those of the Fe^{III} and Cr^{III} ions in $[Fe(CN)_6]^{3-}$ and $[Cr(CN)_6]^{3-}$ building blocks, which have a standard octahedral geometry. The Cr–C≡N and Cr–N≡O bond angles are essentially linear [172.1(3)–176.7(3)°], whereas the Mn–N≡C bond angles deviate markedly from linearity [147.8(2)° for Mn(1)–N(5)–C(5), 148.0(2)° for Mn(1)$^{\#}$–N(3)–C(3) (symmetry operation: $^{\#}$ –*x* + 1/2, *y* + 1/2, –*z* + 3/2), 148.2(3)° for Mn(2)–N(2)–C(2), and 157.5(3)° for Mn(3)–N(4)–C(4)], and give rise to a wave-like chain structure (Table 2).

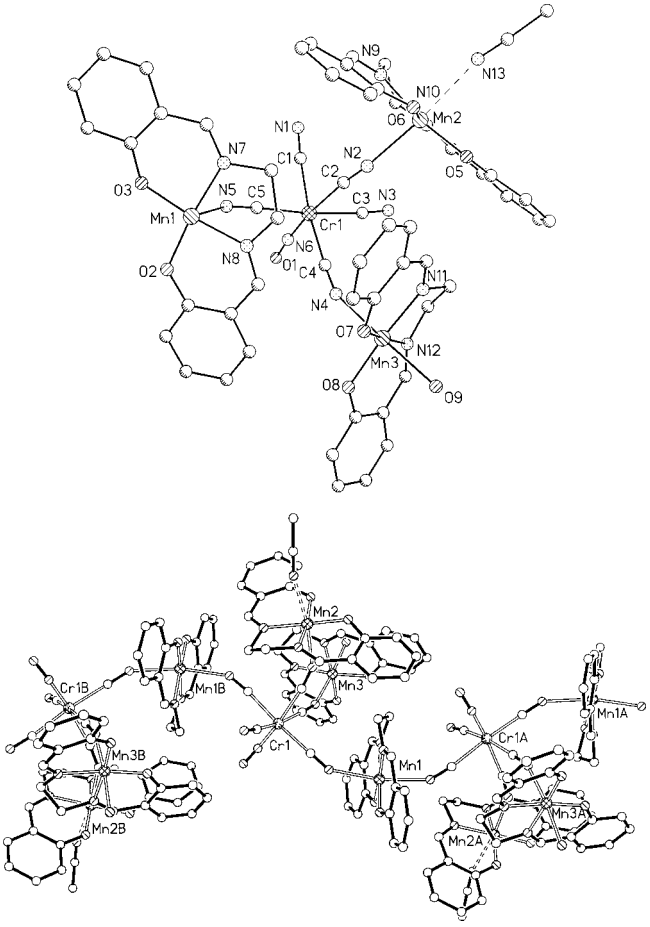

Figure 2. Tetrameric building unit (top) and the one-dimensional chain-like structure (bottom) in complex **2**.

Interestingly, two adjacent chains along the *a* axis arrange oppositely and form relatively broad cavities where the dangling $[Mn(salen)]^+$ units [Mn(2) and Mn(3)] are ac-

Table 2. Selected bond lengths [Å] and angles [°] for **2**.[a]

Mn(1)–N(5)	2.333(3)	Mn(2)–N(2)	2.206(3)	Mn(3)–N(4)	2.240(3)
Mn(1)–N(3)$^{\#1}$	2.296(3)	Mn(2)–N(9)	1.981(3)	Mn(3)–N(11)	1.979(3)
Mn(1)–N(7)	1.987(3)	Mn(2)–N(10)	1.974(3)	Mn(3)–N(12)	1.977(3)
Mn(1)–N(8)	1.991(3)	Mn(2)–O(5)	1.866(2)	Mn(3)–O(7)	1.861(2)
Mn(1)–O(2)	1.885(2)	Mn(2)–O(6)	1.871(2)	Mn(3)–O(8)	1.888(2)
Mn(1)–O(3)	1.879(2)	Mn(2)–N(13)	2.605(5)	Mn(3)–O(9)	2.331(3)
Cr(1)–C(1)	2.049(4)	Cr(1)–C(2)	2.111(3)	Cr(1)–C(3)	2.068(3)
Cr(1)–C(4)	2.052(3)	Cr(1)–C(5)	2.066(3)	Cr(1)–N(6)	1.695(3)
C(1)–N(1)	1.149(4)	C(2)–N(2)	1.147(4)	C(3)–N(3)	1.138(4)
C(4)–N(4)	1.151(4)	C(5)–N(5)	1.151(4)	N(6)–O(1)	1.188(4)
Mn(1)–N(5)–C(5)	147.8(2)	Mn(2)–N(2)–C(2)	148.2(3)	Mn(3)–N(4)–C(4)	157.5(3)
Mn(1)$^{\#2}$–N(3)–C(3)	148.0(3)	Cr(1)–C(1)–N(1)	175.8(3)	Cr(1)–C(2)–N(2)	172.5(3)
Cr(1)–C(3)–N(3)	172.1(3)	Cr(1)–C(4)–N(4)	176.1(3)	Cr(1)–C(5)–N(5)	176.7(3)
Cr(1)–N(6)–O(1)	176.1(3)				

[a] Symmetry operations: $^{\#1}$ $-x + 1/2$, $y - 1/2$, $-z + 3/2$; $^{\#2}$ $-x + 1/2$, $y + 1/2$, $-z + 3/2$.

commodated, whereas the Mn(1) units are situated in the formed narrow cavities and afford the shortest interchain metal–metal distance of 8.040 Å (Figure 3).

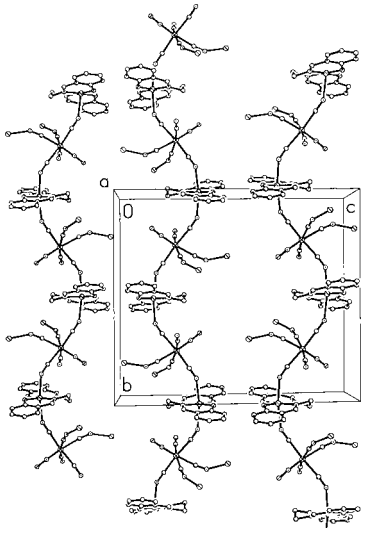

Figure 3. Cell-packing diagram of complex **2** showing the wave-like chain structure along the *a* axis [only the Mn^{III} ions of the dangling Mn(salen) units are shown].

Unlike complex **2**, the structure of **3** consists of an anionic chain formed by a $[Cr(CN)_5(NO)]^{3-}$ and two $[Mn(5\text{-Br-salen})]^+$ units (see Figure 4 and Supporting Information), with a free $[Mn(5\text{-Br-salen})(H_2O)(MeOH)]^+$ moiety as the countercation. Three *mer*-cyanido groups of $[Cr(CN)_5(NO)]^{3-}$ in the chain are linked to the $[Mn(5\text{-Br-salen})]^+$ units. One $[Mn(5\text{-Br-salen})]^+$ and one $[Cr(CN)_5(NO)]^{3-}$ unit connect alternately through two *cis*-cyanido groups in $[Cr(CN)_5(NO)]^{3-}$ to give rise to a zigzag primary chain; another $[Mn(5\text{-Br-salen})(MeOH)]^+$ unit dangles outside the $Mn^{III}Cr^{I}$ chain. The free $[Mn(5\text{-Br-salen})(H_2O)(MeOH)]^+$ countercations are in the vicinity of the anionic chains. The Mn–$N_{cyanido}$ bond lengths are 2.230(11) Å for Mn(1)–N(1), 2.251(12) Å for Mn(2)–N(2), and 2.281(11) Å for Mn(2)–N(3)$^{\#}$ (symmetry operation: $^{\#}$ $-x + 1/2$, $y - 1/2$, $-z + 1/2$). The Mn–N≡C bond angles are 138.1(10)° for Mn(1)–N(1)–C(1), 160.7(12)° for Mn(2)–N(2)–C(2), and 145.6(11)° for Mn(2)$^{\#}$–C(3)–N(3) (symmetry operation: $^{\#}$ $-x + 1/2$, $y + 1/2$, $-z + 1/2$), with an average value of 148.1(11)° (Table 3).

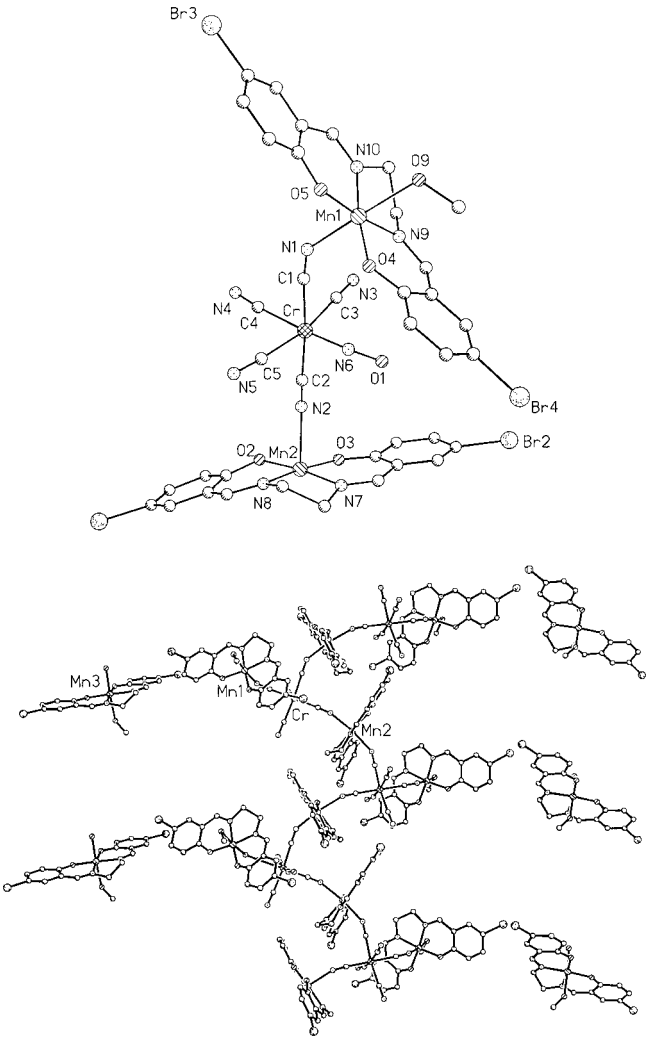

Figure 4. Top: one unit of the chain {the free $[Mn(5\text{-Br-salen})(H_2O)(CH_3OH)]^+$ block is omitted for clarity}; bottom: one-dimensional zigzag chain structure in complex **3**.

Table 3. Selected bond lengths [Å] and angles [°] for **3**.[a]

Mn(1)–N(1)	2.230(11)	Mn(2)–N(2)	2.251(12)	Mn(3)–N(11)	2.006(11)
Mn(1)–N(9)	1.971(10)	Mn(2)–N(3)$^{\#1}$	2.281(11)	Mn(3)–N(12)	1.988(10)
Mn(1)–N(10)	1.971(9)	Mn(2)–N(7)	2.007(9)	Mn(3)–O(6)	1.881(8)
Mn(1)–O(4)	1.890(7)	Mn(2)–N(8)	1.995(9)	Mn(3)–O(7)	1.878(9)
Mn(1)–O(5)	1.881(9)	Mn(2)–O(2)	1.892(7)	Mn(3)–O(8)	2.310(11)
Mn(1)–O(9)	2.332(8)	Mn(2)–O(3)	1.888(7)	Mn(3)–O(2w)	2.241(9)
Cr(1)–C(1)	2.084(15)	Cr(1)–C(2)	2.098(14)	Cr(1)–C(3)	2.040(13)
Cr(1)–C(4)	2.087(13)	Cr(1)–C(5)	2.064(13)	Cr(1)–N(6)	1.687(10)
C(1)–N(1)	1.152(14)	C(2)–N(2)	1.106(14)	C(3)–N(3)	1.155(14)
C(4)–N(4)	1.143(14)	C(5)–N(5)	1.152(14)	N(6)–O(1)	1.178(11)
Cr(1)···Mn(1)	5.324	Cr(1)···Mn(2)	5.213	Cr(1)···Mn(2)$^{\#2}$	5.228
Mn(1)–N(1)–C(1)	138.1(10)	Mn(2)–N(2)–C(2)	160.7(12)	Mn(2)$^{\#2}$–N(3)–C(3)	145.6(11)
Cr(1)–C(1)–N(1)	173.0(11)	Cr(1)–C(2)–N(2)	176.0(13)	Cr(1)–C(3)–N(3)	178.8(12)
Cr(1)–C(4)–N(4)	174.6(12)	Cr(1)–C(5)–N(5)	175.2(11)	Cr(1)–N(6)–O(1)	168.2(11)

[a] Symmetry operations: $^{\#1}$ $-x + 1/2, y - 1/2, -z + 1/2$; $^{\#2}$ $-x + 1/2, y + 1/2, -z + 1/2$.

The zigzag chains form a 2D structure with alternating saddle-like squares through H-bonds between the free cyanido nitrogen atoms and the coordinated methanol oxygen atoms (see Supporting Information). This 2D layered structure is further linked by the free (Schiff base)Mn^{III} units through H-bonds involving cyanido nitrogen, phenoxy oxygen, and coordinated water to form a 3D network structure. Since the adjacent chains are linked together by N···H–O H-bonds (N···O = 2.775 Å), the closest interchain metal–metal distance is only 6.722 Å for Mn–Cr, which is much shorter than that in complex **2** (8.040 Å).

The out-of-plane phenoxido-bridged dimeric $[Mn(saltmen)]_2^{2+}$ cations found in complex **4** connect $[Cr(CN)_5(NO)]^{3-}$ in a *trans* fashion to give rise to a 2D network structure with free ClO_4^- as counteranion. The layered structure of **4** is very similar to that of the complex $[\{Mn(saltmen)\}_4\{Fe(CN)_6\}]ClO_4\cdot H_2O$[12] reported by Miyasaka et al. It is worth noting that a cyclic dodecanuclear square unit is formed through alternating dimeric $[Mn(saltmen)]_2^{2+}$ and $[Cr(CN)_5(NO)]^{3-}$ groups. Figure 5 shows the pentanuclear $[\{Mn(saltmen)\}_4\{Cr(CN)_5(NO)\}]^+$ moiety and the 2D network structure along the *c* axis (Table 4).

The Mn^{III} ion in the complex has a distorted octahedral geometry in which the equatorial plane is occupied by N_2O_2 donor atoms from the saltmen^{2-} ligand while the two *trans* positions are taken up by the cyanido nitrogen and the phenoxy oxygen atom [O(2)$^{\#}$] of the adjacent (Schiff base) Mn^{III} unit (symmetry operation: $^{\#}$ $1/2 + x, 1/2 + y, z$). The $Mn–N_{cyanido}$ bond length is 2.166(9) Å for Mn(1)–N(1) and the corresponding Mn–N≡C bond angle is 154.6(8)° for Mn(1)–N(1)–C(1). The Mn(1)–O(2)$^{\#}$ bond length is 2.629(11) Å, comparable to those of $[\{Mn(saltmen)\}_4\{Fe(CN)_6\}]ClO_4\cdot H_2O$ [2.847(9) Å] and the dimeric precursor $[Mn(saltmen)(H_2O)]_2(ClO_4)_2$ [2.434(2) Å]. The Mn···Mn distance in the dimeric unit is 3.474(8) Å. The Mn···Cr distance through the cyanido ligand is 5.231(8) Å and the shortest interlayer metal–metal separation is 11.879(8) Å.

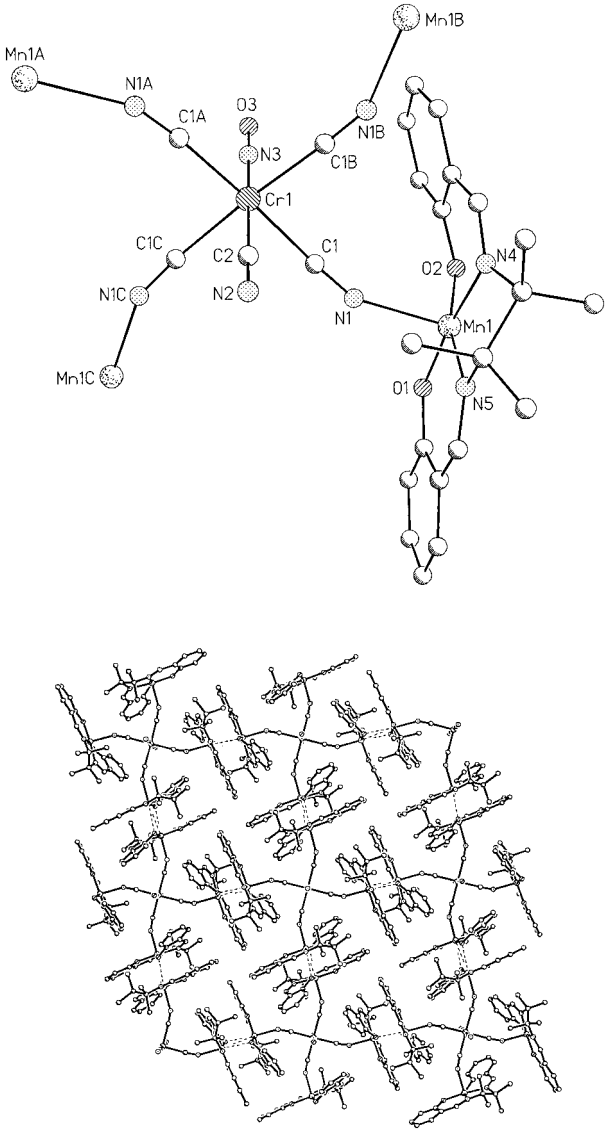

Figure 5. Pentanuclear Mn_4Cr unit (top) and the two-dimensional network structure (bottom) in complex **4** (broken lines represent the weak axial phenoxido–Mn^{III} coordination).

Table 4. Selected bond lengths [Å] and angles [°] for **4**.

Mn(1)–N(1)	2.166(9)	Mn(1)–N(4)	1.987(9)	Mn(1)–N(5)	1.967(10)
Mn(1)–O(1)	1.883(6)	Mn(1)–O(2)	1.892(8)	Cr(1)–C(1)	2.061(11)
Cr(1)–C(2)	2.06(3)	Cr(1)–N(3)	1.74(2)	N(1)–C(1)	1.160(12)
C(2)–N(2)	1.17(3)	O(3)–N(3)	1.19(2)	Cr(1)···Mn(1)	5.230
Mn(1)–N(1)–C(1)	154.6(8)	Cr(1)–C(1)–N(1)	175.2(9)	Cr(1)–C(2)–N(2)	180.000(2)
O(3)–N(3)–Cr(1)	180.0				

Magnetic Properties

The temperature-dependence of $\chi_m T$ for **1** is shown in Figure 6. Upon cooling, the $\chi_m T$ value decreases smoothly from 300 to 40 K before increasing again. The maximum of the curve is at 20 K, with a $\chi_m T$ value of 8.380 emu K mol^{-1}. The origin of the decrease in $\chi_m T$ (below 20 K) may be due to the saturation effect and the zero-field-splitting (ZFS) effect of Mn^{III}. The magnetic susceptibilities (25–300 K) obey the Curie–Weiss law with a negative Weiss constant, θ, of –8.8 K and a Curie constant, C, of 9.425(1) emu K mol^{-1}, which also confirms the presence of an overall antiferromagnetic interaction in **1**.

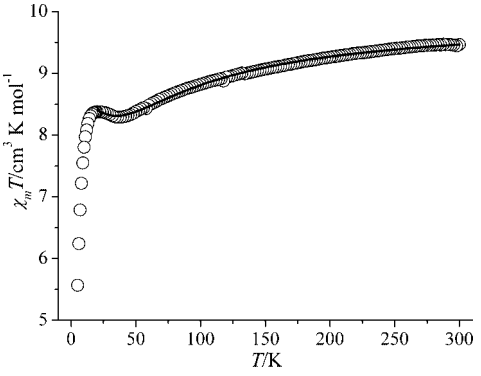

Figure 6. Temperature dependence of $\chi_m T$ for **1**. The solid line represents the theoretical results based on the parameters described in the text.

On the basis of the trinuclear model, the magnetic susceptibilities can be fitted by the expression given in Equation (1) derived from the isotropic exchange spin Hamiltonian $\hat{H} = -2J\hat{S}_{Cr}[\hat{S}_{Mn(1)} + \hat{S}_{Mn(2)}] - 2J'\hat{S}_{Mn(1)}\hat{S}_{Mn(2)}$ for an Mn_2Cr trinuclear unit ($S_{Mn} = 2$, $S_{Cr} = 1/2$) by neglecting the bond-angle difference of Mn–N≡C for simplicity, where $A = 165 + 84\exp(-9J/kT) + 84\exp(-J/kT - 8J'/kT) + 35\exp(-8J/kT - 14J'/kT) + 35\exp(-2J/kT - 14J'/kT) + 10\exp(-7J/kT - 14J'/kT) + 10\exp(-3J/kT - 18J'/kT) + \exp(-6J/kT - 18J'/kT) + \exp(-4J/kT - 10J'/kT)$, and $B = 20 + 16\exp(-9J/kT) + 16\exp(-J/kT - 8J'/kT) + 12\exp(-8J/kT - 14J'/kT) + 12\exp(-2J/kT - 14J'/kT) + 8\exp(-7J/kT - 14J'/kT) + 8\exp(-3J/kT - 18J'/kT) + 4\exp(-6J/kT - 18J'/kT) + 4\exp(-4J/kT - 20J'/kT)$.

$$\chi_t = \frac{Ng^2\beta^2}{kT}\left[\frac{A}{B}\right] \quad (1)$$

The final molar magnetic susceptibility (χ_m/Mn_3Cr) takes the form of Equation (2).

$$\chi_m = \chi_t + \frac{Ng_{Mn}^2\beta^2}{3kT} S_{Mn}(S_{Mn}+1) \quad (2)$$

The best-fit parameters obtained are $J = -10.4$ cm^{-1}, $g = g_{Mn} = 2.06$, $J' = -1.29$ cm^{-1} and $R = \sum(\chi_{obsd}T - \chi_{calcd}T)^2/\sum(\chi_{obsd}T)^2 = 3.75 \times 10^{-5}$ in the temperature range 20–300 K. We note that the absolute J value is much larger than that (ca. –2 cm^{-1}) for the antiferromagnetically coupled Mn^{III}–Fe^{III} analogues,[11] which is indicative of the presence of a stronger magnetic interaction between Mn^{III} and Cr^{I}.

The temperature dependence of the $\chi_m T$ product per Mn_3Cr unit in the range 2–300 K for **2** is shown in Figure 7. The room-temperature $\chi_m T$ values are in good agreement with the expected value of 9.375 emu K mol^{-1} (calculated by assuming $g = 2.0$) for one low-spin Cr^{I} and three high-spin Mn^{III} ions. Upon cooling, the $\chi_m T$ value of **2** decreases smoothly from 300 to 70 K and then increases, with a maximum value of 27.5 emu K mol^{-1} at 4.3 K. The negative Weiss constant of –8.78(10) K and a Curie constant of 9.385(1) emu K mol^{-1} can be obtained from the data between 5 and 300 K. These indicate that the Mn^{III}–Cr^{I} magnetic coupling through the cyanido bridges is antiferromagnetic. The decrease in $\chi_m T$ below 4.3 K suggests the presence of interchain antiferromagnetic coupling (see below).

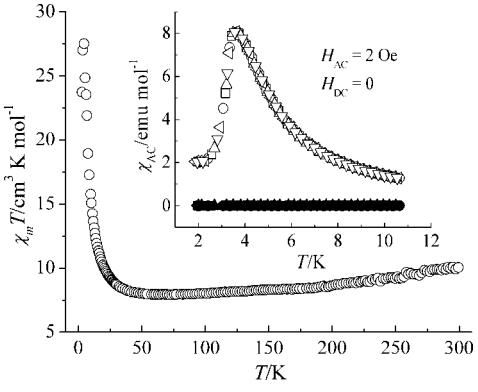

Figure 7. Temperature dependence of $\chi_m T$ for **2**. Inset: temperature dependence of the AC magnetization for **2** in zero static field and an AC field of 2 Oe at 111, 199, 355, 633 and 1111 Hz.

The field-cooled magnetization (FCM) and zero-field-cooled magnetization (ZFCM) plots for **2** (see Supporting Information) at an applied field, H, of 100 Oe show a maximum at around 3.6 K, which demonstrates that there is an antiferromagnetic phase transition at this temperature. The real part of the AC magnetic susceptibility displayed in the

inset of Figure 7 also has a maximum at around 3.6 K, and the imaginary part is zero, which suggests that the critical temperature (T_N) is approximately 3.6 K.

The field-dependence of the magnetization and the hysteresis loop measured at 1.83 K (see Supporting Information) show a spin transition from antiferromagnetic to ferromagnetic. A critical field of 500 Oe is observed. This metamagnetic behavior is commonly observed for 2D layered antiferromagnets with short-range, intralayer ferri- or ferromagnetic ordering.[31–35]

The temperature-dependence of the $\chi_m T$ magnetic behavior of **3** is similar to that of **1** and **2**, as shown in Figure 8. Upon cooling, $\chi_m T$ decreases smoothly, reaching a minimum at 80 K, and then increases. The maximum of the curve is at 9.2 K, with a $\chi_m T$ value of 12.1 emu K mol^{-1}. The magnetic susceptibilities above 10 K obey the Curie–Weiss law with a negative Weiss constant of –4.98(6) K and a Curie constant of 9.257(1) emu K mol^{-1}, which also confirms the presence of overall antiferromagnetic interactions in **3**.

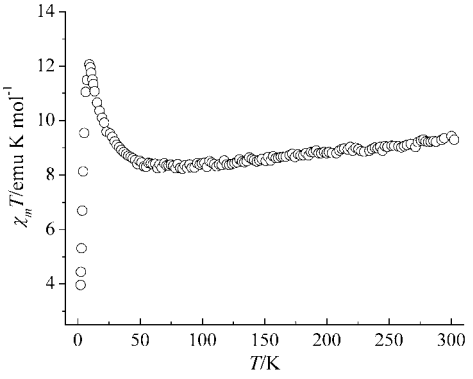

Figure 8. Temperature dependence of $\chi_m T$ for **3**.

The temperature dependence of the magnetic susceptibility in a zero DC and 3-Oe AC magnetic field for complex **3** is displayed in Figure 9. The out-of-phase AC magnetic susceptibility has nonzero values below 4.0 K and is strongly frequency-dependent. The shift of the peak temperature (T_P) of χ'' is evaluated by the parameter $\Phi = (\Delta T_P/T_P)/\Delta(\log\omega) = 0.17$, which is larger than that for a canonical spin-glass but smaller than the normal value for a superparamagnet.[36–39] The hysteresis loop at 1.8 K shows noticeable magnetic hysteresis (Figure 10), which indicates the presence of magnetic ordering in complex **3**.

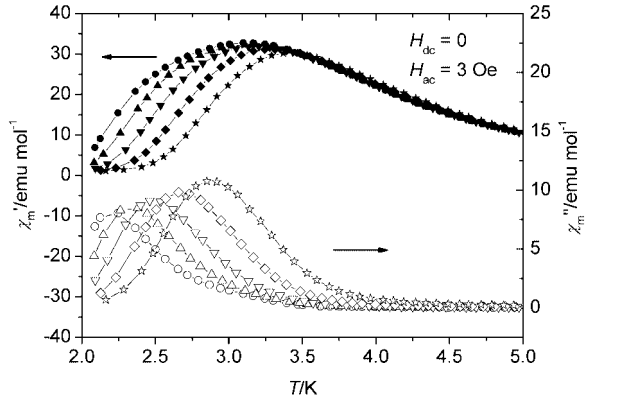

Figure 9. Temperature dependence of the AC magnetization for **3** in a zero static field and an AC field of 3 Oe at frequencies of 277 (circles), 666 (triangles tip up), 1633 (tringles tip down), 4111 (diamonds), and 9999 (stars) Hz.

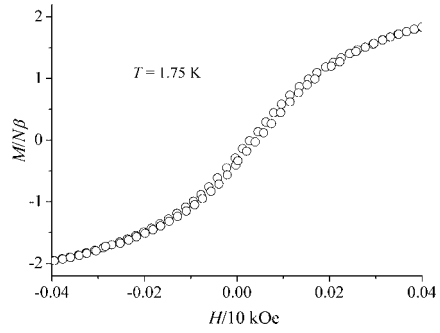

Figure 10. Magnetic hysteresis loop for **3** at 1.75 K.

The crystal data show that there is a large number of strong H-bonds in complex **3** which form a 3D network structure and that the metal···metal distance is 6.722 Å. This suggests the presence of a significant intermolecular magnetic interaction. Therefore, we tentatively attribute the slow relaxation of magnetization in **3** to a spin-glass behavior.[39] The origin of this spin-glass behavior may be due to the presence of competitive ferro- and antiferromagnetic coupling within the chains considering the presence of a wide range of cyanido bridging bond angles [138.1(10)–160.7(12)°].

The magnetic susceptibilities of complex **4** were measured in the temperature range 2–300 K in an applied magnetic field of 2000 Oe. The plot of $\chi_m T$ vs. T for **4** is shown in Figure 11, where χ_m is the magnetic susceptibility per Mn_4Cr unit. The room-temperature $\chi_m T$ value of 12.541 emu K mol^{-1} is nearly equal to the spin-only value of 12.375 emu K mol^{-1} for five uncoupled spins [four S_{Mn} (S = 2) and one S_{Cr} (S = 1/2)]. On lowering the temperature, $\chi_m T$ decreases gradually to 11.82 emu K mol^{-1} at 150 K, then increases smoothly until about 50 K before rapidly reaching a maximum value of 166 emu K mol^{-1} at 8 K, and then sharply decreases to 56.5 emu K mol^{-1} at 2 K, which

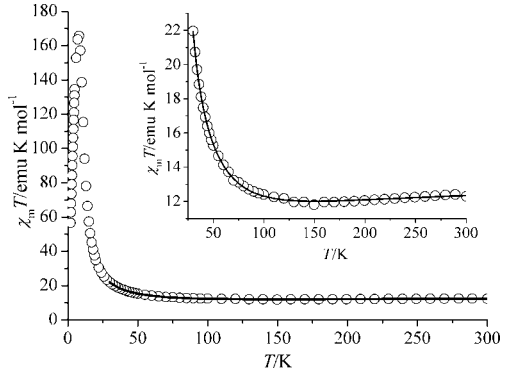

Figure 11. Temperature dependence of $\chi_m T$ for **4**. Inset: enlarged view in the temperature range 25–300 K. The solid line shows the best fit based on the parameters discussed in the text.

suggests the presence of global antiferromagnetic interactions and three-dimensional magnetic ordering in the complex. The plot of $1/\chi_m$ vs. T above 150 K obeys the Curie–Weiss law with a negative Weiss constant of –12.5 K and a Curie constant of 12.4 emu K mol^{-1}, which suggest that antiferromagnetic coupling between Mn^{III} and Cr^{I} through a cyanido bridge is dominant in the high-temperature range with the Mn^{III}–Mn^{III} ferromagnetic coupling through the phenoxido bridges superimposed. The higher temperature shift of the minimum in $\chi_m T$ for **4** (150 K) than those of complexes **1**–**3** (40 K for **1**, and 70 for **2**, and 80 K for **3**) may be due to the presence of ferromagnetic Mn^{III}–Mn^{III} interactions through the phenoxy oxygen atoms.

To evaluate the magnitude of the intramolecular magnetic coupling, we tried to fit the magnetic susceptibilities to the model previously employed for coordination polymers.[20] The structural information shows that in complex **4** there are two different magnetic coupling pathways, namely cyanido bridges and phenoxido bridges. The layers are illustrated schematically in Scheme 2, where J is for the cyanido bridges and J' for the phenoxido ones. We can see from the $\chi_m T$ vs. T plot that J is dominant, i.e. $|J| >> |J'|$. The 2D layer can be accordingly described as weakly interacting Mn_4Cr pentanuclear units in which an antiferromagnetic coupling ($J < 0$) is present.

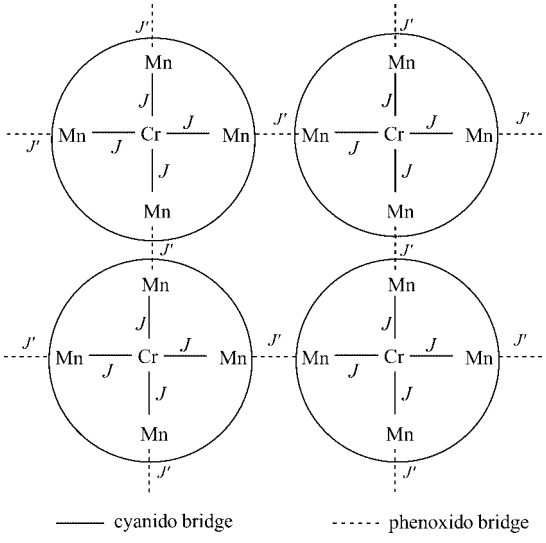

Scheme 2. Schematic view of the layer structure of **4** showing the magnetic coupling pathways.

Based on the above considerations, the magnetic data were fitted to the Van Vleck equation for the pentanuclear unit derived from the exchange Hamiltonian $\hat{H} = -2J\hat{S}_{Cr}(\hat{S}_{Mn1} + \hat{S}_{Mn2} + \hat{S}_{Mn3} + \hat{S}_{Mn4})$.[11,15] The magnetic coupling through the phenoxido bridges was treated as an intermolecular term using the mean-field method. The final molar magnetic susceptibility (χ_m) is in the form of Equation (3), where χ_p is for the Mn_4Cr pentanuclear unit, J' is the coupling constant between the pentanuclear units, and z, the number of nearest Mn_4Cr neighbors, is 4. Other symbols have their usual meanings.

$$\chi_m = \chi_p/[1 - \chi_p(2zJ'/Ng^2\beta^2)] \quad (3)$$

The best-fit parameters based on the data above 30 K are $J = -17.2$ cm^{-1}, $zJ' = 0.17$ cm^{-1}, $g_{Mn} = 1.97$, and $g_{Cr} = 3.70$. The calculated solid line shown in Figure 11 agrees well with the experimental values. The calculated J value is comparable to that [–10.4(1) cm^{-1}] for the trinuclear Mn_2Cr compound **1**. The positive J' value suggests a ferromagnetic Mn^{III}–Mn^{III} coupling through the phenoxido bridges. However, this value is smaller than that for the similar Mn_2 complexes according to the equation $J' = 4.5724 - 1.1868x$ (x is the Mn–$O_{phenoxido}$ distance [Å] in the range of 2.4–3.7 Å) proposed by Miyasaka et al.[40] This may be due to the rough approximation of the fit. Furthermore, the g_{Cr} value is too large, although the use of a value less than 3.0 did not give a satisfactory fit. Nevertheless, the g_{Cr} value is not reasonable, and should be considered with care.

To further confirm the magnetic phase transition, the temperature dependence of the AC magnetic susceptibility was measured at a zero DC and a 5-Oe AC field, as shown in Figure 12. The real part of the AC magnetic susceptibility has a maximum peak at about 6.4 K which is accompanied by the occurrence of a nonzero χ_{AC}'', thereby suggesting that the T_c of complex **4** is about 6.4 K, similar to that of the 2D analogue [{Mn(saltmen)}$_4${Fe(CN)$_6$}]-$ClO_4 \cdot H_2O$[12] (4.5 K). The hysteresis loop at 2.0 K (see Supporting Information) displays a characteristic behavior for a soft ferromagnet, with a small coercive field of 10 Oe and a remnant magnetization of about 4.0 $N\beta$.

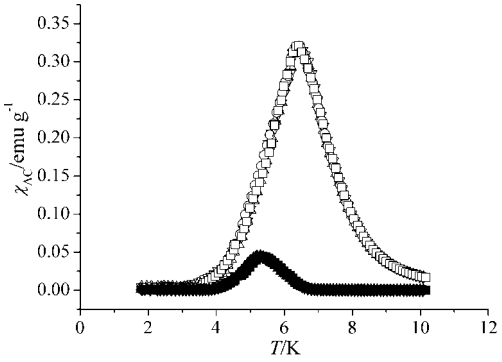

Figure 12. Temperature dependence of the AC magnetization for **4** in a zero static field and an AC field of 2 Oe at 277, 666, 1633, and 4111 Hz.

The nature of the magnetic coupling between the high-spin Mn^{III} ion (d^4, t_{2g}^3, e_g^1) and the low-spin Cr^{I} ion (d^5, t_{2g}^5) through the cyanido bridge should be similar to those of cyanido-bridged Mn^{III}–$Fe^{III}(CN)_6$ systems.[11,12,14] According to the GK rule,[41] ferromagnetic and antiferromagnetic contributions coexist, and the antiferromagnetic contributions that originate from the overlap of magnetic orbitals of t_{2g} symmetry between Mn^{III}–Fe^{III} and Mn^{III}–Cr^{I} are dominant in these systems. Therefore, overall antiferromagnetic interactions between Mn^{III} and Cr^{I} through cyanido groups are expected for complexes **1**–**4** in this work, as is also observed in the 3D Prussian blue analogue Mn^{III}-$[Cr(CN)_5(NO)] \cdot H_2O$ recently reported by Liao et al.[42] In

addition, the bending of the Mn–N≡C angle is an important factor that affects the magnetic coupling in these systems because it diminishes the overlap of t_{2g}-type magnetic orbitals on adjacent metal ions and therefore weakens the antiferromagnetic contributions. It has been concluded empirically that an Mn–N≡C angle close to 150° tends to favor ferromagnetic coupling in cyanido-bridged Mn^{III}–Fe^{III} systems.[14] However, the magnetic couplings for the cyanido-bridged Mn^{III}–Cr^{I} systems in this work are all antiferromagnetic, with average Mn–N≡C angles in the range 148.1(11)–158.7(6)°, therefore further work needs to be done to fully elucidate the nature of the magnetic interactions in cyanido-bridged Mn^{III}–Cr^{I} systems.

Conclusions

Polynuclear 1D and 2D Mn^{III}–Cr^{I} complexes have been synthesized by tuning the Schiff-base ligands around Mn^{III}. The complexes in the present work all show antiferromagnetic Mn^{III}–Cr^{I} coupling, which is in contrast to the $[Fe(CN)_6]^{3-}$ analogues, which usually exhibit intermetallic ferromagnetic interactions.[11–16,19–23] In this regard, $[Cr(CN)_5(NO)]^{3-}$ is much like $[Cr(CN)_6]^{3-}$, as no ferromagnetic cyanido-bridged Mn^{III}–Cr^{III} complexes have been found so far.[43] The present study further demonstrates that this is a good strategy for designing and assembling molecule-based magnetic materials based on (Schiff base)Mn^{III} precursors and cyanido-bearing paramagnetic building blocks.

Experimental Section

General Remarks: Elemental analyses for carbon, hydrogen, and nitrogen were carried out with an Elementar Vario EL. The IR spectra were recorded with a Magna-IR 750 spectrophotometer in the region 4000–650 cm^{-1}. Variable-temperature magnetic susceptibility measurements of **1**–**4** were performed with a Quantum Design MPMS SQUID magnetometer. The zero-field AC magnetic susceptibilities of **1**, **3**, and **4** were recorded with a MagLab 2000 magnetometer. The experimental susceptibilities were corrected for the diamagnetism of the constituent atoms (Pascal's tables).

General Procedures for the Synthesis of (Schiff Base)Mn^{III} Complexes: The precursors [Mn(salen)]ClO_4, [Mn(5-Br-salen)]ClO_4, [Mn(5-Cl-salen)]ClO_4, and [Mn(saltmen)]ClO_4 were synthesized according to the following procedure. Solid $[Mn(ClO_4)_2]\cdot 6H_2O$ (1.8 g, 5 mmol) was added to an MeOH and EtOH solution (40 mL, MeOH/EtOH = 1:1, v/v) of the Schiff base H_2salen (1.34 g, 5 mmol), H_2-5-Cl-salen (1.7 g, 5 mmol), H_2-5-Br-salen (2.1 g, 5 mmol), or H_2saltmen (1.6 g, 5 mmol), then solid NaOH (5 mmol) was added directly to the above mixture whilst stirring at room temperature. The mixture was then warmed to about 60–70 °C and kept at this temperature for about 1–3 h until the solid Schiff base had completely dissolved and the solution had become dark red/brown. After cooling and filtering, the solution was kept at room temperature for several days, which gave rise to red/brown crystals in high yield (80%).

Synthesis of Complexes 1–3: Red/brown crystals of **1**, **2**, and **3** were obtained at room temperature by the slow diffusion of a yellow aqueous solution (5 mL) of $K_3[Cr(CN)_5(NO)]\cdot H_2O$ (0.1 mmol, 32.9 mg) into a reddish brown mixture of [Mn(5-Cl-salen)]ClO_4 (0.2 mol, 98.4 mg), [Mn(salen)]ClO_4 (0.2 mol, 84.4 mg), or [Mn(5-Br-salen)]ClO_4 (0.2 mol, 116 mg) in MeOH and MeCN (5 mL) over about one week. These crystals were collected carefully and air-dried. Yield: 10–15%. IR: **1**: ν(C≡N) 2114 m, ν(N≡O) 1687 m, ν(C=N) 1628 cm^{-1} vs; **2**: ν(C≡N) 2113 m, 2246 w (CH_3CN), ν(N≡O) 1677 s, ν(C=N) 1625 cm^{-1} vs; **3**: ν(C≡N) 2009 m, ν(N≡O) 1684 s, ν(C=N), 1627 cm^{-1} vs. **1**: $C_{53}H_{43}Cl_6CrMn_3N_{12}O_{10.50}$ (1445.5): calcd. C 44.04, H 3.00, N 11.63; found C 44.79, H 2.96, N 11.35; **2**: $C_{56.50}H_{54}CrMn_3N_{13.50}O_{10.50}$ (1307.0): calcd. C 51.92, H 4.16, N 14.47; found C 51.37, H 4.13, N 14.22; **3**: $Mn_3CrC_{55}H_{50}Br_6N_{12}O_{12}$ (1767.4): calcd. C 37.38, H 2.85, N 9.51; found C 37.30, H 2.86, N 8.98.

Synthesis of Complex 4: Thin lamellar brown single crystals of **4** suitable for X-ray structure analysis were grown at room temperature by slow evaporation of an MeOH/MeCN/H_2O solution of [Mn(saltmen)]ClO_4 (64.9 mg, 0.2 mmol) and $K_3[Cr(CN)_5(NO)]\cdot H_2O$ (32.0 mg, 0.1 mmol) for several days. Yield: 28 mg (30% based on Mn). IR: ν(C≡N) 2114 m, ν(N≡O) 1712 s, ν(C=N) 1602 cm^{-1}

Table 5. Crystal data for complexes **1**–**4**.

	1	**2**	**3**	**4**
Empirical formula	$C_{53}H_{43}Cl_6CrMn_3N_{12}O_{10.50}$	$C_{56.50}H_{54}CrMn_3N_{13.50}O_{10.50}$	$C_{55}H_{50}CrBr_6Mn_3N_{12}O_{12}$	$C_{85}H_{88}ClCrMn_4N_{14}O_{16}$
Fomula mass	1445.51	1306.95	1767.35	1868.90
T [K]	123	293	293	123
Crystal system	rhombohedral	monoclinic	monoclinic	tetragonal
Space group	$R\bar{3}$	$P2_1/n$	$P2_1/n$	$I4/m$
a [Å]	35.000(5)	11.822(2)	15.770(4)	18.613(3)
b [Å]	35.000(5)	19.0635(8)	13.486(3)	18.613(3)
c [Å]	27.442(6)	22.1293(9)	31.048(8)	27.738(6)
α [°]	90	90	90	90
β [°]	90	96.777(1)	97.77(2)	90
γ [°]	120	90	90	90
V [Å^3]	29112(8)	6085.3(4)	6542(3)	9610(3)
Z	18	4	4	4
$\rho_{calcd.}$ [g cm^{-3}]	1.484	1.427	1.794	1.292
F(000)	13140	2682	3476	3860
Data/restraints/parameters	22777/1/1481	10676/0/802	9102/6/800	3847/3/287
GOF on F^2	0.956	1.003	0.998	1.078
R_1 [$I > 2\sigma(I)$]	0.0741	0.0494	0.0744	0.1429
wR_2 (all data)	0.1859	0.1482	0.2134	0.2771

vs. $C_{85}H_{88}ClCrMn_4N_{14}O_{16}$ (1868.9): calcd. C 54.63, H 4.75, N 10.49; found C 54.25, H 4.68, N 10.26.

X-ray Structure Determination: Data collection for **2** was performed with a Simens Bruker P4 diffractometer, that for **3** with a Bruker Smart CCD, and that for **1** and **4** with a Rigaku Saturn70 CCD diffractometer (123 K). The structures were solved by direct methods with SHELXS-97 and refined by full-matrix least squares (SHELXL-97) on F^2. Hydrogen atoms were added geometrically and refined using a riding model. One free MeCN molecule in complex **2** and one CN^- and one NO^- group from one $[Cr(CN)_5(NO)]^{3-}$ unit in complex **1** are disordered over two sets of positions. Single crystals of **4** are thin, weakly diffracting, and give high final R values: $R_1 = 0.1429$, $wR_2 = 0.2771$ (all data). Its molecular structure was further confirmed by elemental analysis and magnetism studies. Crystallographic data for complexes **1**–**4** are summarized in Table 5. CCDC-623479 to -623482 (**1**–**4**, respectively) contain the supplementary crystallographic data for this paper. These data can be obtained free of charge from The Cambridge Crystallographic Data Center via www.ccdc.cam.ac.uk/data_request/cif.

Supporting Information (see footnote on the first page of this article): Schematic view of the structures of **1** and **4**; cell packing diagrams for **1**–**4**; FCM and ZFCM plots, hysteresis loop, and magnetization data at 1.83 K for **2**; hysteresis loop at 2.0 K for **4**; powder XRD plot for complex **4**.

Acknowledgments

This work was supported by the Ministry of Science Technology, China through a 973 Project (no. 2002CB613301) and the Fok Ying Tong Education Foundation.

[1] a) S. Ferlay, T. Mallah, R. Ouahès, P. Veillet, M. Verdaguer, *Nature* **1995**, *378*, 701–703; b) W. R. Entley, G. S. Girolami, *Science* **1995**, *268*, 397–400; c) S. M. Holmes, G. S. Girolami, *J. Am. Chem. Soc.* **1999**, *121*, 5593–5594; d) O. Hatlevik, W. E. Buschmann, J. L. Manson, J. S. Miller, *Adv. Mater.* **1999**, *11*, 914–918; e) H.-Z. Kou, S. Gao, J. Zhang, G.-H. Wen, G. Su, R. K. Zheng, X. X. Zhang, *J. Am. Chem. Soc.* **2001**, *123*, 11809–11810.

[2] a) M. Ohba, H. Ōkawa, *Coord. Chem. Rev.* **2000**, *198*, 313–328; b) K. Inoue, H. Imai, P. S. Ghalsasi, K. Kikuchi, M. Ohba, H. Okawa, J. V. Yakhmi, *Angew. Chem. Int. Ed.* **2001**, *40*, 4242–4245; c) T. Kashiwagi, S.-I. Ohkoshi, H. Seino, Y. Mizobe, K. Hashimoto, *J. Am. Chem. Soc.* **2004**, *126*, 5024–5025.

[3] a) T. E. Vos, J. S. Miller, *Angew. Chem. Int. Ed.* **2005**, *44*, 2416–2419; b) T. Glaser, M. Heidemeier, T. Weyhermüller, R.-D. Hoffmann, H. Rupp, P. Müller, *Angew. Chem. Int. Ed.* **2006**, *45*, 2416–2419.

[4] M. Verdaguer, A. Bleuzen, V. Marvaud, J. Vaissermann, M. Seuleiman, C. Desplanches, A. Scuiller, C. Train, R. Garde, G. Gelly, C. Lomenech, I. Rosenman, P. Veillet, C. Cartier, F. Villain, *Coord. Chem. Rev.* **1999**, *190–192*, 1023–1047.

[5] B. Sieklucka, R. Podgajny, T. Korzeniak, P. Przychodzeń, R. Kania, *C. R. Chimie* **2002**, *5*, 639–649.

[6] L. M. C. Beltran, J. R. Long, *Acc. Chem. Res.* **2005**, *38*, 325–334.

[7] R. Lescouëzec, L. Marilena Toma, J. Vaissermann, M. Verdaguer, F. S. Delgado, C. Ruiz-Pérez, F. Lloret, M. Julve, *Coord. Chem. Rev.* **2005**, *249*, 2691–2729.

[8] a) C. P. Berlinguette, D. Vaughn, C. Cañada-Vilalta, J. R. Galán-Mascarós, K. R. Dunbar, *Angew. Chem. Int. Ed.* **2003**, *42*, 1523–1526; b) Y. Song, P. Zhang, X.-M. Ren, X.-F. Shen, Y.-Z. Li, X.-Z. You, *J. Am. Chem. Soc.* **2005**, *127*, 3708–3709; c) E. J. Schelter, A. V. Prosvirin, K. R. Dunbar, *J. Am. Chem. Soc.* **2004**, *126*, 15004–15005; d) S. Wang, J.-L. Zuo, H.-C. Zhou, H. J. Choi, Y. Ke, J. R. Long, X.-Z. You, *Angew. Chem. Int. Ed.* **2004**, *43*, 5940–5943; e) D. F. Li, S. Parkin, G. Wang, G. T. Yee, A. V. Prosvirin, S. M. Holmes, *Inorg. Chem.* **2005**, *44*, 4903–4905; f) A. V. Palii, S. M. Ostrovsky, S. I. Klokishner, B. S. Tsukertlat, C. P. Berlinguette, K. R. Dunbar, J. R. Galán-Mascarós, *J. Am. Chem. Soc.* **2004**, *126*, 16860–16867.

[9] a) C. P. Berlinguette, A. Dragulescu-Andrasi, A. Sieber, H.-U. Güudel, C. Achim, K. R. Dunbar, *J. Am. Chem. Soc.* **2005**, *127*, 6766–6779; b) S. Bonhommeau, G. Molnár, A. Galet, A. Zwick, J.-A. Real, J. J. McGarvey, A. Bousseksou, *Angew. Chem. Int. Ed.* **2005**, *44*, 4069–4073; c) M. Nihei, M. Ui, M. Yokota, L. Han, A. Maeda, H. Kishida, H. Okamoto, H. Oshio, *Angew. Chem. Int. Ed.* **2005**, *44*, 6484–6487.

[10] a) O. Sato, T. Iyoda, A. Fujishima, K. Hashimoto, *Science* **1996**, *272*, 704–705; b) O. Sato, T. Kawakami, M. Kimura, S. Hishiya, S. Kubo, Y. Einaga, *J. Am. Chem. Soc.* **2004**, *126*, 13176–13177; c) V. Escax, G. Champion, M.-A. Arrio, M. Zacchigna, C. C. D. Moulin, A. Bleuzen, *Angew. Chem. Int. Ed.* **2005**, *44*, 4798–4801; d) T. Yamamoto, Y. Umemura, O. Sato, Y. Einaga, *J. Am. Chem. Soc.* **2005**, *127*, 16065–16073; e) J. G. Moore, E. J. Lochner, C. Ramsey, N. S. Dalal, A. E. Stiegman, *Angew. Chem. Int. Ed.* **2003**, *42*, 2741–2743.

[11] H. Miyasaka, H. Ieda, N. Matsumoto, N. Re, R. Crescenzi, C. Floriani, *Inorg. Chem.* **1998**, *37*, 255–263.

[12] H. Miyasaka, N. Matsumoto, H. Ōkawa, N. Re, E. Gallo, C. Floriani, *J. Am. Chem. Soc.* **1996**, *118*, 981–994.

[13] H. J. Choi, J. J. Sokol, J. R. Long, *Inorg. Chem.* **2004**, *43*, 1606–1608.

[14] H. Miyasaka, H. Takahashi, T. Madanbashi, K.-I. Sugiura, R. Clérac, H. Nojiri, *Inorg. Chem.* **2005**, *43*, 5969–5971.

[15] S.-F. Si, J.-K. Tang, Z.-Q. Liu, D.-Z. Liao, Z.-H. Jiang, S.-P. Yan, P. Cheng, *Inorg. Chem. Commun.* **2003**, *6*, 1109–1112.

[16] H. J. Choi, J. J. Sokol, J. R. Long, *J. Phys. Chem. Solids* **2004**, *65*, 839–844; T. Glaser, M. Heidemeier, T. Weyhermuller, R.-D. Hoffmann, H. Rupp, P. Muller, *Angew. Chem. Int. Ed.* **2006**, *45*, 6033–6037.

[17] X. Shen, B. Li, J. Zou, Z. Xu, Y. Yu, S. Liu, *Transition Met. Chem.* **2002**, *27*, 372–376.

[18] X. Shen, B. Li, J. Zou, H. Hu, Z. Xu, *J. Mol. Struct.* **2003**, *657*, 325–331.

[19] a) N. Re, E. Gallo, C. Floriani, H. Miyasaka, N. Matsumoto, *Inorg. Chem.* **1996**, *35*, 6004–6008; b) H.-R. Wen, C.-F. Wang, Y.-Z. Li, J.-L. Zuo, X.-Z. You, *Inorg. Chem.* **2006**, *45*, 7032–7034.

[20] M. Ferbinteanu, H. Miyasaka, W. Wernsdorfer, K. Nakata, K. Sugiura, M. Yamashita, C. Coulon, R. Clérac, *J. Am. Chem. Soc.* **2005**, *127*, 3090–3099.

[21] H. Miyasaka, H. Ieda, N. Matsumoto, K.-I. Sugiura, M. Yamashita, *Inorg. Chem.* **2003**, *42*, 3509–3515.

[22] H. Miyasaka, N. Matsumoto, N. Re, E. Gallo, C. Floriani, *Inorg. Chem.* **1997**, *36*, 670–676.

[23] H. Miyasaka, H. Okawa, A. Miyazaka, T. Enoki, *Inorg. Chem.* **1998**, *37*, 4878–4883.

[24] N. Matsumoto, Y. Sunatsuki, H. Miyasaka, Y. Hashimoto, D. Luneau, J.-P. Tuchagues, *Angew. Chem. Int. Ed.* **1999**, *38*, 171–173.

[25] Z.-H. Ni, H.-Z. Kou, L.-F. Zhang, C. Ge, A.-L. Cui, R.-J. Wang, Y. Li, O. Sato, *Angew. Chem. Int. Ed.* **2005**, *44*, 7742–7745.

[26] P. Przychodzeń, K. Lewinski, M. Balanda, R. Pełka, M. Rams, T. Wasiutynshi, C. Guyard-Duhayon, B. Sieklucka, *Inorg. Chem.* **2004**, *43*, 2967–2974.

[27] P. Przychodzeń, M. Rams, C. Guyard-Duhayon, B. Sieklucka, *Inorg. Chem. Commun.* **2005**, *8*, 350–354.

[28] H.-Z. Kou, Z.-H. Ni, B. C. Zhou, R.-J. Wang, *Inorg. Chem. Commun.* **2004**, *7*, 1150–1153.

[29] Y. Kim, S.-M. Park, S.-J. Kim, *Inorg. Chem. Commun.* **2002**, *5*, 592–595.

[30] M. Clemente-León, E. Coronado, J. R. Galán-Mascarós, C. J. Gómez-García, Th. Woike, J. M. Clemente-Juan, *Inorg. Chem.* **2001**, *40*, 87–94.
[31] a) E. Colacio, J. M. Dominguez-Vera, M. Ghazi, R. Kivekas, F. Lloret, J. M. Moreno, H. Stoeckli-Evans, *Chem. Commun.* **1999**, 987–988; b) E. Colacio, M. Ghazi, H. Stoeckli-Evans, F. Lloret, J.-M. Moreno, C. Perez, *Inorg. Chem.* **2001**, *40*, 4876–4883; c) Z. Shen, J.-L. Zuo, F.-N. Shi, Y. Xu, Y. Song, X.-Z. You, S. S. S. Raj, H. K. Fun, Z.-Y. Zhou, C. M. Che, *Transition Met. Chem.* **2001**, *26*, 345–350.
[32] H. Xiang, S. Gao, T. B. Lu, R. L. Luck, Z. W. Mao, X. M. Chen, L. N. Ji, *New J. Chem.* **2001**, *25*, 875–878.
[33] a) H.-Z. Kou, S. Gao, W.-M. Bu, D.-Z. Liao, B.-Q. Ma, Z.-H. Jiang, S.-P. Yan, Y.-G. Fan, G.-L. Wang, *J. Chem. Soc., Dalton Trans.* **1999**, 2477–2480; b) H.-Z. Kou, W.-M. Bu, S. Gao, D.-Z. Liao, Z.-H. Jiang, S.-P. Yan, Y.-G. Fan, G.-L. Wang, *J. Chem. Soc., Dalton Trans.* **2000**, 2996–2999.
[34] A. Marvilliers, S. Parsons, E. Riviere, J. P. Audiere, M. Kurmoo, T. Mallah, *Eur. J. Inorg. Chem.* **2001**, 1287–1293.
[35] H.-Z. Kou, S. Gao, O. Bai, Z.-M. Wang, *Inorg. Chem.* **2001**, *40*, 6287–6294.
[36] H. Miyasaka, R. Clerac, K. Mizushima, K.-i. Sugiura, M. Yamashita, W. Wernsdorfer, C. Coulon, *Inorg. Chem.* **2003**, *42*, 8203–8213.
[37] R. Lescouezec, J. Vaissermann, C. Ruiz-Perez, F. Lloret, R. Carrasco, M. Julve, M. Verdaguer, Y. Dromzee, D. Gatteschi, W. Wernsdorfer, *Angew. Chem. Int. Ed.* **2003**, *42*, 1483–1485.
[38] T.-F. Liu, D. Fu, S. Gao, Y.-Z. Zhang, H.-L. Sun, G. Su, Y.-J. Liu, *J. Am. Chem. Soc.* **2004**, *125*, 13976–13977.
[39] J. Kim, S. Han, K. I. Pokhodnya, J. M. Migliori, J. S. Miller, *Inorg. Chem.* **2005**, *44*, 6983–6988.
[40] H. Miyasaka, R. Clerac, T. Ishii, H.-C. Chang, S. Kitagawa, M. Yamashita, *J. Chem. Soc., Dalton Trans.* **2002**, 1528–1534.
[41] a) J. B. Goodenough, *Phys. Rev.* **1955**, *100*, 564–573; b) J. Kanamori, *J. Phys. Chem. Solids* **1959**, *10*, 87–98.
[42] H.-B. Zhou, W. Zhang, K. Yoshimura, Y. Ouyang, D.-Z. Liao, Z.-H. Jiang, S.-P. Yan, P. Cheng, *Chem. Commun.* **2005**, 4979–4981.
[43] An argument has been made to assign the oxidation state of Cr in $[Cr(CN)_5(NO)]^{3-}$ as +3: M. Ardon, S. Cohen, *Inorg. Chem.* **1993**, *32*, 3241–3243.

Received: October 13, 2006
Published Online: February 14, 2007

